

Artificial intelligence applications in Parkinson's disease via retinal imaging

Ali Jafarizadeh ^{1,*,#}, Hamidreza Ashayeri ^{2,#}, Hadi Vahedi ¹, Parsa Khalafi ³, Mirsaeed Abdollahi ¹, Navid Sobhi ⁴, Ru-San Tan ^{5,6}, Roohallah Alizadehsani ^{7,*}, U. Rajendra Acharya ^{8,9}

1. Nikookari Eye Center, Tabriz University of Medical Sciences, Tabriz, Iran.
2. Research Center for Evidence-based Medicine, Iranian EBM Center: A Joana-affiliated group, Tabriz University of Medicine Science, Tabriz, Iran
3. School of Medicine, Tehran University of Medical Sciences, Tehran, Iran
4. Translational Ophthalmology Research Center, Farabi Eye Hospital, Tehran University of Medical Science, Tehran, Iran.
5. National Heart Centre Singapore, Singapore.
6. Duke-NUS Medical School, Singapore.
7. Institute for Intelligent Systems Research and Innovation (IISRI), Deakin University, VIC 3216, Australia
8. School of Mathematics, Physics and Computing, University of Southern Queensland, Springfield, Australia
9. Centre for Health Research, University of Southern Queensland, Australia

*Corresponding Authors:

1- Roohallah Alizadehsani, PhD

Institute for Intelligent Systems Research and Innovation (IISRI), Deakin University, VIC 3216, Australia

Tel: +61 3 524 79394

Postal: 75 Pigdons Rd, Waurn Ponds VIC 3216, Australia

Email: r.alizadehsani@deakin.edu.au

<https://orcid.org/0000-0003-0898-5054>

2- Ali Jafarizadeh, MD, MPH

Nikookari Eye Center, Tabriz University of Medical Sciences, Tabriz, Iran

Tel: +98 901 098 0062

Postal code: 51666/14766

Email: Jafarizadeha@tbzmed.ac.ir; Ali.jafarizadeh.md@gmail.com

<https://orcid.org/0000-0003-4922-1923>

Author details:

Name	Degree	Email	ORCID
Ali Jafarizadeh	MD, MPH	ali.jafarizadeh.md@gmail.com	https://orcid.org/0000-0003-4922-1923
Hamidreza Ashayeri	MD	hashayeri97@gmail.com	https://orcid.org/0000-0002-2593-9810
Hadi Vahedi	MD	Hadivahedimrg@gmail.com	https://orcid.org/0009-0008-4769-451X
Parsa Khalafi	MD, MSc	p-khalafi@alumnus.tums.ac.ir	https://orcid.org/0009-0005-1975-9855
Mirsaeed Abdollahi	MD	abdollahi.mirsaeed@gmail.com	https://orcid.org/0000-0002-2444-1172
Navid Sobhi	MD	navidsbg.ns1998@gmail.com	https://orcid.org/0000-0003-0663-850X
Ru-San tan	MBBS	tanrshc@gmail.com.sg	https://orcid.org/0000-0003-2086-6517
Roohallah Alizadehsani	PhD	r.alizadehsani@deakin.edu.au	https://orcid.org/0000-0003-0898-5054
U. Rajendra Acharya	PhD, DEng, DSc	Rajendra.Acharya@unisq.edu.au	https://orcid.org/0000-0003-2689-8552

Abstract

Parkinson's disease (PD) is projected to increase substantially due to population aging, making early diagnosis increasingly important, as timely detection may delay progression and reduce long-term complications. Retinal microvasculature has emerged as a promising anatomical biomarker of neurodegeneration, and when combined with artificial intelligence AI, retinal imaging may provide an advanced, noninvasive, and cost-effective screening strategy for PD. This study evaluated the evidence from the past 35 years regarding the capability of AI to detect early PD-related changes in retinal vascular structure. Five electronic databases including PubMed, Web of Science, Scopus, ScienceDirect, and ProQuest were systematically searched from January 1990 to January 2025. In addition, *Annals of Neurology* and *Frontiers in Neuroscience* were hand-searched, and the reference lists of included studies were screened for additional eligible publications. Nineteen studies met the inclusion criteria. Three principal diagnostic AI tasks were identified, including disease classification, retinal vessel segmentation, and PD risk stratification. The best-performing models were ShAMBi-LSTM on the Drishti dataset with 97.2 percent accuracy, 99.5 percent precision, 96.9 percent sensitivity, and an F1 score of 0.981 for classification, nnU-Net with 99.7 percent accuracy, 98.7 percent precision, 98.9 percent sensitivity, 99.8 percent specificity, and a Dice score of 98.9 percent for segmentation, and AlexNet for risk prediction with area under the curve values of 0.77, 0.68, and 0.73 across datasets. Overall, application of AI algorithms to retinal vasculature for detecting early signs of PD and predicting disease severity suggests that integration of AI with retinal biomarkers holds substantial potential for earlier and more accurate detection compared with traditional clinical evaluation alone.

Keywords: Artificial intelligence, Parkinson's disease, Retinal imaging, Microvasculature, Deep learning.

Highlights:

1. Early thinning of RNFL and GCL is a key non-invasive retinal biomarker for PD.
2. AI analysis of retinal imaging can detect early PD, segment retinal layers, and estimate disease severity.
3. AI performance depends heavily on data quality, architecture choice, and advanced methods (TL and XAI)
4. The top-performing AI algorithms in different tasks were ShAMBi-LSTM for classification, nnU-Net for segmentation, and AlexNet for risk prediction.

1. Introduction

Parkinson's disease (PD) is a neurodegenerative disease affecting nearly 12 million people worldwide (Luo et al., 2025). PD incidence increases with age; only 4% of cases are less than 50 years old (Van Den Eeden et al., 2003). With global population aging, the prevalence of PD is estimated to increase by 76% from 2021 to 2050 (Su et al., 2025). Early diagnosis is crucial, as timely detection and management can delay progression and reduce long-term complications. Clinical diagnosis of PD is based on detailed history and neurological examination. It is important to exclude neurological conditions that mimic PD (Kobylecki, 2020) using neuroimaging, e.g., magnetic resonance imaging (MRI) (Heim et al., 2017; Pyatigorskaya et al., 2014). Accurate diagnosis enables appropriate management, but the task is onerous and requires expertise. There is an unmet need for accessible screening tools for population-level detection of PD.

Retinal imaging has been proposed as a cost-effective solution for PD screening. The retina undergoes distinct structural and functional changes in PD. PD severity and duration are negatively associated with retinal ganglion cell inner plexiform (GCL-IPL) and ganglion cell complex (GCC) thicknesses (Bayhan et al., 2014; Sari et al., 2015). The close relationship between retinal and central nervous system (CNS) pathologies is implied by several studies. Simultaneously, in PD, there are numerous degenerative, dysfunctional, and structural retinal changes. PD duration is negatively correlated with retinal nerve fiber layer (RNFL) thickness, and the Unified Parkinson's Disease Rating Scale (UPDRS) is negatively correlated with light-adapted electroretinography findings (Elanwar et al., 2023). Notably, retinal imaging data are amenable to artificial intelligence (AI)-enabled analysis. Both machine learning (ML) and deep learning (DL) are increasingly being applied in medical imaging to perform various tasks, such as image segmentation, artifact detection, quality improvement, and image classification (Thrall et al., 2018). This work reviews published research on AI applications for various aspects of PD detection using retinal imaging (Figure 1).

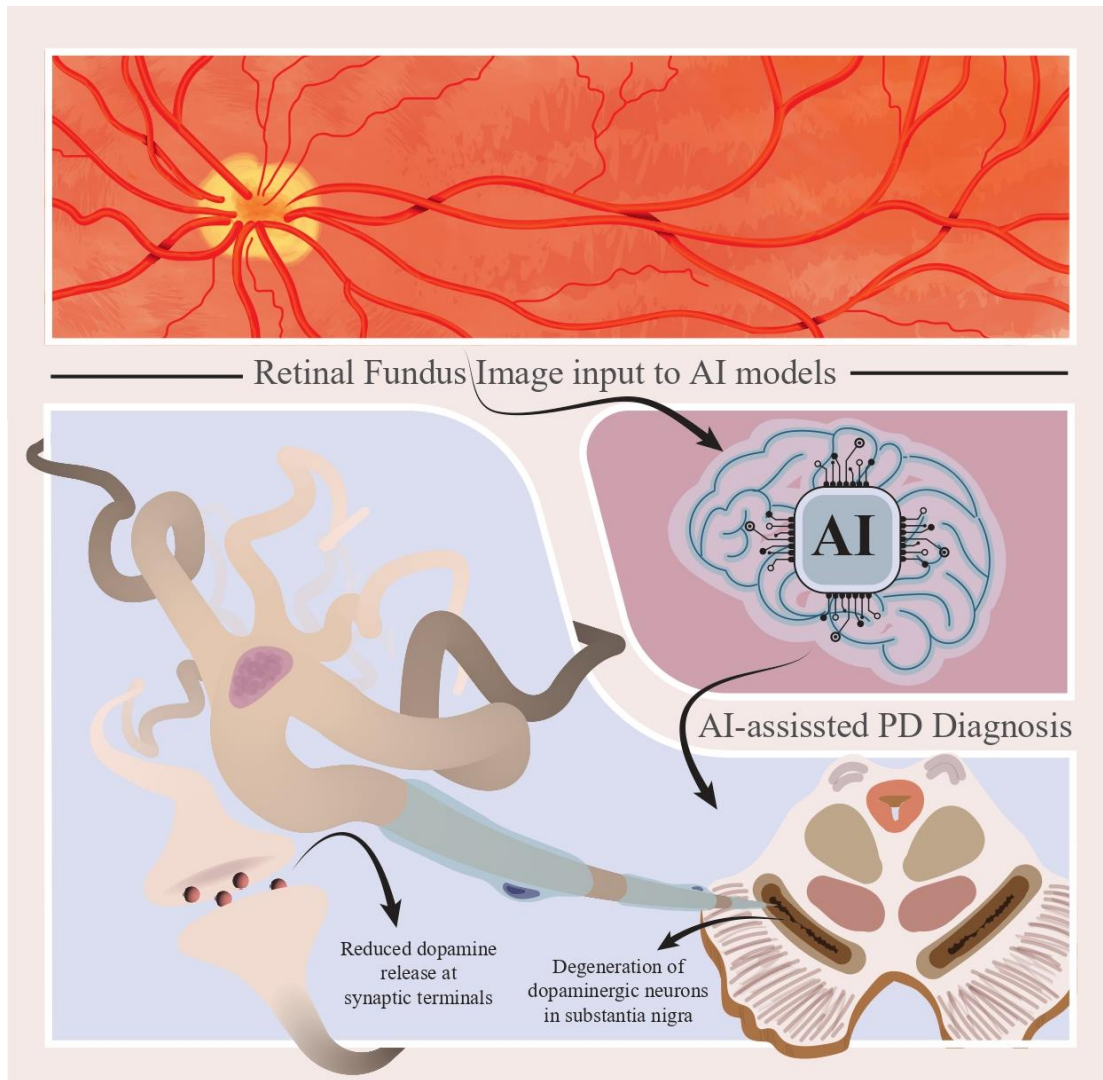


Figure 1. AI applications in Parkinson's disease detection through retinal imaging.

2. Method

We performed a literature search for articles published between January 1990 to January 2025 in PubMed, Web of Science (WOS), Scopus, ScienceDirect, and ProQuest. We included original research that employed ML or DL for the prediction and diagnosis of PD in patients, including image processing (e.g., image segmentation) of retinal images obtained by different methods, such as funduscopy and optical coherence tomography (OCT). We excluded review studies, book chapters, editorials, letters, studies that did not use ML or DL, studies that did not include patients with PD, studies that did not use retinal images,

and studies that did not contain at least an extended English abstract. The Boolean strings used for searching the different databases are detailed in Table S1. Using the same inclusion and exclusion criteria, we performed a hand search of articles published within the same period in two key journals, “Annals of Neurology” and “Frontiers in Neuroscience”. References of selected studies were also scanned for suitable studies. Table 1 summarizes the inclusion and exclusion criteria used to during the selection of papers.

Table 1. Inclusion and exclusion criteria employed to select the papers.

Inclusion criteria	Exclusion criteria
Original studies that use: <ul style="list-style-type: none"> • Machine learning or Deep learning algorithms and • Retinal images obtained by different methods, such as fundoscopy or optical coherence tomography • For prediction, diagnosis, and image segmentations • In patients with Parkinson`s disease 	<ul style="list-style-type: none"> • Review studies/ Book chapters/ Editorials/ Letters • Studies that didn`t use Machine learning/Deep learning • Studies that didn`t include patients with Parkinson`s disease • Studies that didn`t use retinal images • Studies without at least an extended English Abstract

3. Results

3.1 Study Selection

A total of 3,323 records were identified across all sources. 1,336 duplicate studies were removed, leaving 1,987 studies. Screening of abstracts, followed by full-text assessment, results in a final selection of 19 studies (Ahn et al., 2023; Álvarez-Rodríguez et al., 2024; Chen et al., 2024; Chrysou et al., 2024; Gende et al., 2023; Hu et al., 2025; Hu et al., 2022; J. Huang et al., 2024; Lee et al., 2023; LIANG Keke, 2024; Nunes et al., 2019; Richardson et al., 2024; Rupavath et al., 2024; Shi et al., 2024; Tran et al., 2024; Ueda et al., 2024; Varghese et al., 2023; Zhang et al., 2024; Zhao et al., 2021; Zhou et al., 2023) (Figure 2). Scanning the references of selected studies did not identify any more eligible studies. In a similar study to ours, Ganji et al. (Ganji et al., 2025), aimed to assess the use of AI in detecting multiple neurodegenerative

diseases based on retinal imaging. However, they have included 4 articles with PD patients and we aim to assess the 19 articles used in more extreme detail compared to Ganji et al. (Ganji et al., 2025).

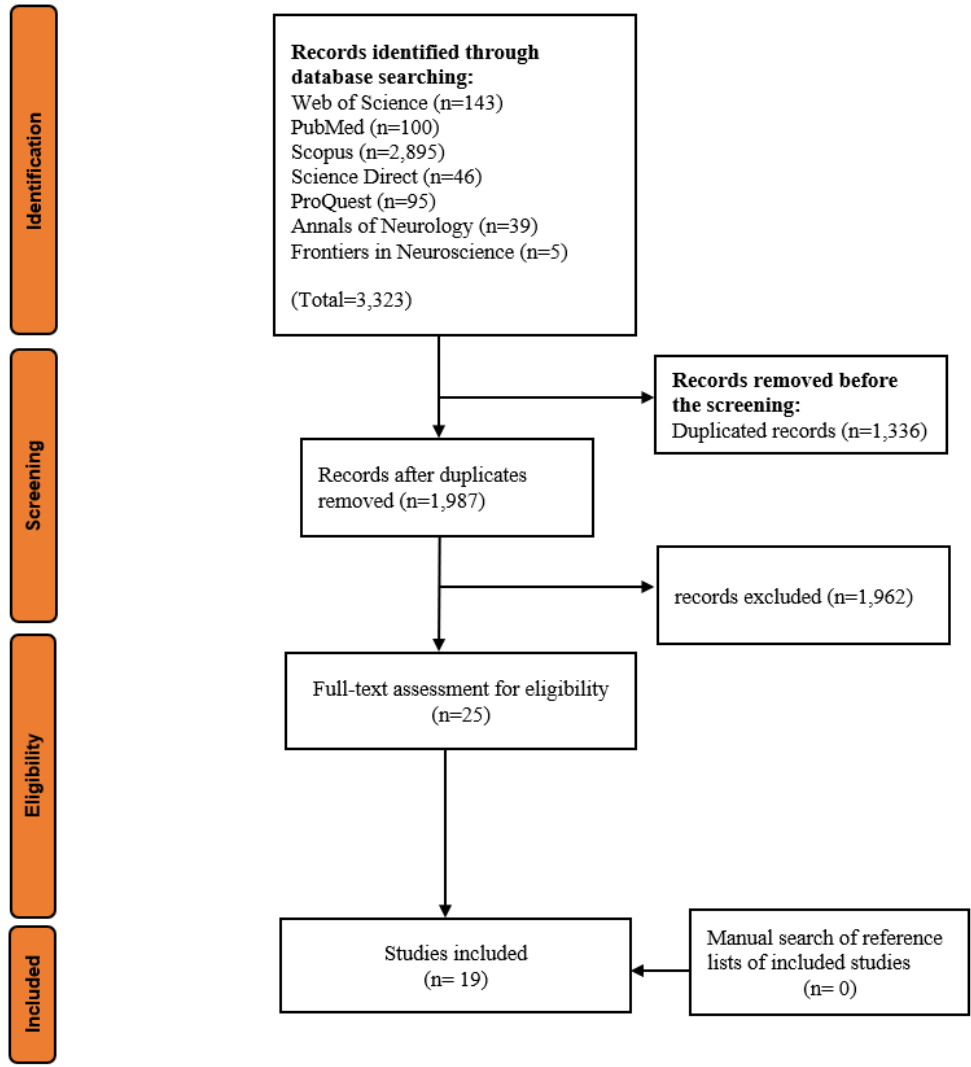


Figure 2. Flow diagram of study selection.

3.2 Study Characteristics

Table 2 summarizes the 19 selected studies. Most datasets were single-center and internally validated; only two studies (Ahn et al., 2023; Zhou et al., 2023) reported a clear external validation cohort. Several papers reported multi-class tasks involving PD patients as well as healthy controls and/or patients with other neurologic or ocular diseases (e.g., Alzheimer’s disease, multiple sclerosis, glaucoma). Included

studies were published during 2019-2025. Figure 3 represents the number of published articles in each year based on their approach (ML or DL). The PD sample sizes in the studies ranged from 6 (Zhang et al., 2021; Zhao et al., 2021) to 322 (Zhou et al., 2023) patients, with most studies enrolling 20–150 PD subjects; several papers also included healthy controls and/or other neurologic or ocular diseases (e.g., AD, MS, glaucoma) to enable multi-class tasks or differential diagnosis. 9 (47.3%) studies used OCT alone (Álvarez-Rodríguez et al., 2024; Chen et al., 2024; Chrysou et al., 2024; Gende et al., 2023; Jingqi Huang et al., 2024; Nunes et al., 2019; Shi et al., 2024; Zhang et al., 2024; Zhao et al., 2021); 5 (26.3%) studies used color fundus photography (Ahn et al., 2023; Hu et al., 2025; Hu et al., 2022; Tran et al., 2024; Varghese et al., 2023); and one evaluated retinal hyperspectral imaging (Ueda et al., 2024). A few studies were multimodal (Lee et al., 2023; Richardson et al., 2024; Zhou et al., 2023), and one article didn't specify which type of retinal image they used from the online datasets (Rupavath et al., 2024).

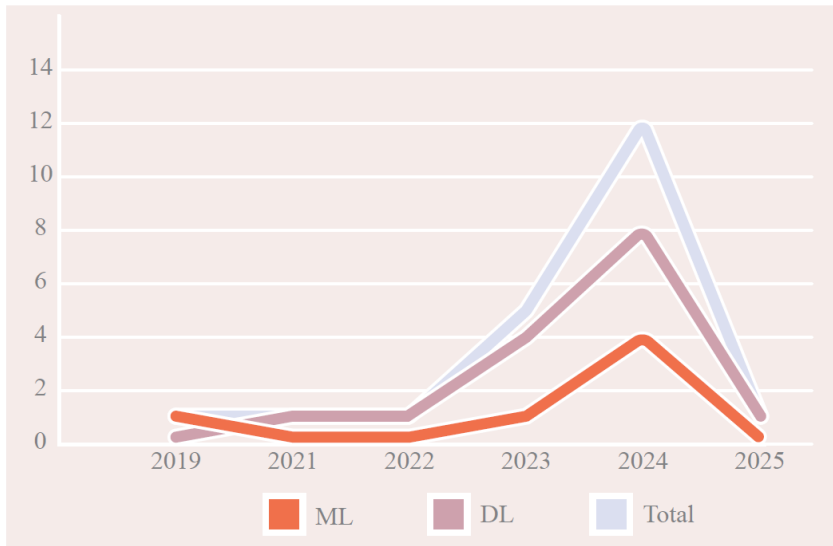


Figure 3. Number of published articles in each year in various categories.

1 **Table 2.** Summary of characteristics of included studies.

Author (Year)	Number of subjects (F/M ratio)	Mean Age \pm Std	Number of used eye images (R/L ratio)	Retinal imaging techniques	Training/ Validation/ Testing (K-fold cross-validation)	Task	AI model	AUC	Accuracy/Precision	Sensitivity/Specificity	Dice score/F1 score
Nunes et al. (2019) (Nunes et al., 2019)	HC: 27 (14/13) PD: 28 (15/13) AD: 20 (10/10)	HC: 64.1 \pm 7.1 PD: 63.4 \pm 6.6 AD: 66.3 \pm 6.8	HC: 53 (26/27) PD: 54 (27/27) AD: 39 (20/19)	OCT	(2, 5, 10-fold cross-validation)	Classification: HC vs PD vs AD (2-fold cross-validation)	SVM	-	76.7% / -	HC: 84.9% / 80.6% PD: 74.1% / 96.7% AD:71.8% / 90.7%	-
						Classification: HC vs PD vs AD (5-fold cross-validation)		-	80.8% / -	HC: 87.7% / 83.9% PD: 75.9% / 97.8% AD:79.5% / 92.5%	-
						Classification: HC vs PD vs AD (10-fold cross-validation)		-	82.2% / -	HC: 88.7% / 84.9% PD: 77.8% / 97.8% AD:79.5% / 92.5%	-
Zhao et al. (2021) (Zhao et al., 2021)	HC: 32 (20/12) PD: 6 (4/2) WMH: 31 (12/19)	HC: 60.56 \pm 5.72 PD: 62.67 \pm 11.48 WMH: 63.58 \pm 7.12	HC: 58 (28/30) PD: 11 (5/6) WMH: 56 (28/28)	OCT	-	Segmentation	CE-Net (Gu et al., 2019)	-	-	-	-
Hu et al. (2022) (Hu et al., 2022)	46886 (female to male ratio of 35834 PD free used for analysis)	Mean age of 35834 patients used for analysis: 56.7 \pm 8.04	19200 fundus images were used	CFP	11052/-/35834	Prediction (not with AI)	Xception model provided by Zhu et al. (2022) (Zhu et al., 2023)	0.708	-	-	-

	55.7% / 44.3%)		for age prediction								
Ahn et al. (2023) (Ahn et al., 2023)	non-PD atypical motor abnormalities: 349 (236/ 113) PD: 266 (132/ 134)	non-PD atypical motor abnormalities: 70.7 ±7.9 PD: 70.8 ± 8.3	non-PD atypical motor abnormalities: 700 PD: 539	CFP	Data were randomly obtained from 80 people for the validation data set, and the rest for the training data set.	Classification: PD vs non-PD atypical motor abnormalities	ResNet-18	0.76	76.75% / -	77.05% / 76.46%	-
							ResNet-101	0.71	71.18% / -	71.65% / 70.73%	-
							VGG19	0.66	66.30% / -	65.61% / 66.96%	-
							EfficientNet-b0	0.73	73.57% / -	75.11% / 72.05%	-
							EfficientNET-b7	0.68	68.36% / -	69.04% / 67.69%	-
					Model 1: fundus only.	Classification: H-Y severity (3 classes)	ResNet-18	0.66	58.24% / -	76.76% / 52.72%	-
					Model 2: fundus with sex and age data.			0.71	64.80% / -	79.48% / 58.81%	-
					Model 3: fundus with sex, age, diabetes, and hypertension data.			0.72	63.55% / -	79.52% / 59.44%	-
					Model 4: fundus image with sex, age, diabetes, and hypertension data with multimodal method.			0.77	73.38% / -	83.23% / 66.81%	-
					Model 1: fundus only.	Classification: Unified Parkinson's Disease Rating Scale (UPDRS-III) (3 classes)	ResNet-18	0.67	59.43% / -	77.16% / 54.75%	-
					Model 2: fundus with sex and age data.			0.69	62.24% / -	78.93% / 57.67%	-
					Model 3: fundus with sex, age, diabetes, and hypertension data.			0.70	65.31% / -	79.54% / 59.21%	-
Model 4: fundus image with sex, age, diabetes, and	0.77	71.64% / -	82.61% / 65.75%	-							

					hypertension data with multimodal method.						
Gende et al. (2023) (Gende et al., 2023)	Individuals recruited from clinics: HC: 10 PD: 10 AD: 10 Relapsing-remitting Multiple Sclerosis: 10 Essential tremor: 10	-	732 OCT images from Li et al.'s dataset (Li et al., 2021) 1250 retinal images from patients recruited from clinics	OCT	The model was pretrained on 732 OCT images, and in experiment 1, it was trained on four groups (40 patients) and tested on the remaining group (10 patients)	Segmentation (RNFL / trained on whole dataset)	MGU-Net (Li et al., 2021)	-	- / 94.2%	95.7% / -	94.9% / -
						Segmentation (GCL-BM / trained on whole dataset)			- / 98.4%	98.6% / -	98.7% / -
						Segmentation (RNFL / trained on whole dataset except PD)		-	- / 93.8%	95.8% / -	94.8% / -
						Segmentation (GCL-BM / trained on whole dataset except PD)			- / 98.4%	98.7% / -	98.5% / -
						Segmentation (RNFL / trained on HC dataset)		-	- / 93%	95.8% / -	94.3% / -
						Segmentation (RNFL / trained on AD dataset)		-	- / 94.6%	93.8% / -	94.2% / -
						Segmentation (RNFL / trained on MS dataset)		-	- / 93.5%	94.1% / -	93.8% / -
						Segmentation (RNFL / trained on ET dataset)		-	- / 93.9%	94.4% / -	94.1% / -
						Segmentation (GCL-BM / trained on HC dataset)		-	- / 98.7%	98.3% / -	98.5% / -

						Segmentation (GCL-BM / trained on AD dataset)		-	- / 98.2%	98.6% / -	98.4% / -
						Segmentation (GCL-BM / trained on MS dataset)		-	- / 98.3%	98.4% / -	98.4% / -
						Segmentation (GCL-BM / trained on ET dataset)		-	- / 98.9%	98.5% / -	98.7% / -
Lee et al. (2023) (Lee et al., 2023)	PD: 107 Normal cognition: 298 Other diseases: 237	-	OCT: 1465	OCT, OCTA	70%/15%/15%	Classification: Good vs poor image quality (GC-IPL OCT scan)	AlexNet	0.99	97.1% / -	88.9% / 97%	-
	PD: 107 Normal cognition: 425 Other diseases: 239		OCTA: 2689			Classification: Good vs poor image quality (OCTA scan)	AlexNet	0.832	76.4% / -	65.7% / 80.9%	-
Varghese et al. (2023) (Varghese et al., 2023)	HC: 528 PD: 133 AD: 18 Vascular dementia: 528	-	Only left eye images were used.	CFP	60%/-/40%		Inductive logic programming	-	-	-	-
Zhou et al. (2023) (Zhou et al., 2023)	MEHAzEye: 1) Control: 293 (144/149)	-	-	CFP, OCT	904170 CFP images and 736442 OCT were used for construction, MEHAzEye data were used for fine-tuning and internal	Prediction: Incident PD vs non-incident PD	RETFound	0.669	-	-	-

	2: PD: 293 (120/173) UK Biobank: 1) Control: 29 (12/17) 2) PD: 29 (19/10)				validation, and UK Biobank was used for external validation						
Álvarez-Rodríguez (2024) et al. (Álvarez-Rodríguez et al., 2024)	HC: 81 PD: 82 AD: 29 Multiple Sclerosis: 166 Essential tremor: 10	-	-	Single-view and Multiview OCT	70%/10%/20%	Segmentation: RNFL	nnU-Net architecture (Macula view-2D approach)	-	99.8% / 93.7%	96.3% / 99.9%	95.5% / -
						Segmentation: GCL - Bruch's Membrane			99.7% / 98.7%		
						Segmentation: RNFL	nnU-Net architecture (Macula view-3D multi-scale cascade approach)	-	99.7% / 92%	93.4% / 99.9%	94.1% / -
						Segmentation: RNFL			99.6% / 98.4%		
						Segmentation: RNFL	nnU-Net architecture (Macula view-3D full resolution approach)	-	99.8% / 94.6%	95.8% / 99.9%	95.7% / -
						Segmentation: GCL - Bruch's Membrane			99.7% / 98.7%		
						Segmentation: RNFL	nnU-Net architecture (Optic view)	-	98.9% / 90.6%	89.9% / 99.5%	90% / -
						Segmentation: GCL - Bruch's Membrane			97.9% / 93.4%		

						Segmentation: RNFL	Transfer learning (Optic view)	-	99.1% / 91.7%	92.0% / 99.5%	91.6% / -
						Segmentation: GCL - Bruch's Membrane	Transfer learning (Optic view)	-	98.2% / 92.1%	91.6% / 99.0%	91.2% / -
Chen et al. (2024) (Chen et al., 2024)	PD: 45	-	630	OCT	441/-/189	Segmentation of retinal layers	Wavelet Transformer (based on U-net architecture)	-	93.73% / -	-	93.46% / -
Chrysou et al. (2024) (Chrysou et al., 2024)	HC: 100 (54/46)	Median age of (IQR) HC: 62.7 (6.5) PD: 65.1 (8.7) Primary open-angle Glaucoma: 78 (45/33)	-	SD-OCT	141/36/44	Classification: PD vs HC	RF	0.71	57% / -	-	-
	PD: 121 (34/87)				128/32/39	Classification: PD vs primary open-angle glaucoma	RF	0.92	82% / -	-	-
Huang et al. (2024) (J. Huang et al., 2024)	HC: 49 (32/17) PD: 26 (11/15)	HC: 61.61 ± 5.94 PD: 65.73 ± 6.90	HC: 1584 PD: 666	OCT	60%/20%/20% (five-fold cross-validation)	Classification: PD vs HC	Wavelet-based Selection and Recalibration Network (WaveSRNet)	0.7516	74.49% / -	-	- / 0.5676
Keke et al. (2024)* (LIANG Keke, 2024)	PD: 49 HC: 39	PD: 40-79	-	OCT, OCTA	62 training/26 validation	Classification: PD vs HC	LR	0.841	-/-	-	-
							Decision tree	0.806	-/-	-	-
							RF	0.766	-/-	-	-
							KNN	0.764	-/-	-	-
							XGBoost	0.732	-/-	-	-

Richardson et al. (2024) (Richardson et al., 2024)	Control: 249 (184/67) PD: 52 (21/31)	Control: 66.4 ± 9.1 PD: 65.9 ± 9.5	Control: 371 (204/169) PD: 75 (39/36)	OCT, OCTA, UWF color photographs, UWF autofluorescence	355 eyes/ 42 eyes/ 49 eyes	Classification: PD vs HC	CNN (OCTA, GC-IPL, UWF FAF, UWF color - Right eye only)	0.91	-	100% / 85%	-
							CNN (OCTA, GC-IPL, UWF FAF, UWF color - Left eye only)	0.918	-	100% / 85.7%	-
							CNN (OCTA, GC-IPL, UWF FAF, UWF color - Both eyes)	0.861	-	-	-
							CNN (OCTA - Right eye only)	0.711	-	-	-
							CNN (OCTA - Left eye only)	0.811	-	-	-
							CNN (OCTA - Both eyes)	0.650	-	-	-
							CNN (GC-IPL - Right eye only)	0.630	-	-	-
							CNN (GC-IPL - Left eye only)	0.556	-	-	-
							CNN (GC-IPL - Both eyes)	0.625	-	-	-
							CNN (UWF FAF - Right eye only)	0.682	-	-	-

							CNN (UWF FAF - Left eye only)	0.794	-	-	-
							CNN (UWF FAF - Both eyes)	0.855	-	-	-
							CNN (UWF color - Right eye only)	0.798	-	-	-
							CNN (UWF color - Left eye only)	0.838	-	-	-
							CNN (UWF color - Both eyes)	0.805	-	-	-
Shi et al. (2024) (Shi et al., 2024)	HC: 49 PD: 26	-	HC: 1584 PD: 666	OCT	Eye-wise five-fold cross-validation	Classification: PD vs HC (Eye-wise)	RSGA-Net	-	88.21% / 81.28%	81.67% / 90.97%	- / 0.8068
							RSGA-Net-V1	-	87.95% / 83.51%	75.08% / 93.40%	- / 0.7842
					subject-wise five-fold cross-validation	Classification: PD vs HC (Subject-wise)	RSGA-Net	-	83.38% / 61.81%	21.39% / 96.43%	- / 0.2899
							RSGA-Net-V1	-	79.95% / 49.98%	29.17% / 90.64%	- / 0.307
Tran et al. (2024) (Tran et al., 2024)	HC: 84 (35/49) PD: 84 (35/49)	HC: 61.8 ± 5.9 PD: 61.8 ± 5.9	HC: 123 PD: 123	CFP	five-fold stratified cross-validation (3 folds for training, one for validation, and one for testing)	Classification: PD vs HC	LR	0.68	63% / -	66% / 61%	- / 0.64
							Elastic Net	0.67	61% / -	68% / 54%	- / 0.64
							SVM (linear)	0.69	63% / -	65% / 62%	- / 0.64
							SVM (RBF)	0.71	67% / -	76% / 58%	- / 0.7
							AlexNet	0.77	68% / -	76% / 60%	- / 0.68

							VGG-16	0.71	66% / -	85% / 46%	- / 0.7
							GoogleNet	0.69	63% / -	77% / 49%	- / 0.67
							Inception-V3	0.56	54% / -	68% / 40%	- / 0.57
							ResNet-50	0.57	54% / -	52% / 55%	- / 0.45
Zhang et al. (2024) (Zhang et al., 2024)	HC: 31 (20/11) PD: 6 (4/2) WMH: 28 (12/16)	HC: 59.1 ± 6.3 PD: 62.7 ± 11.5 WMH: 64±7.5	HC: 57 (27/30) PD: 11 (5/6) WMH: 51 (25/26)	OCT	The model was trained based on the data of all four devices and then tested on the data of three of the datasets individually.	Segmentation: all retinal layers (Heidelberg Spectralis)	SGA	-	-	-	94.43% / -
						Segmentation: all retinal layers (Optovue RTVue)	SGA	-	-	-	87.67% / -
						Segmentation: all retinal layers (Zeiss Cirrus HD-OCT 5000)	SGA	-	-	-	82.48% / -
Ueda et al. (2024) (Ueda et al., 2024)	Control: 20 (10/10) PD: 20 (7/13)	Control: 70.2 ± 10.5 PD: 71.0 ± 8.4	Control: 20 (16/4) PD: 20 (15/5)	Retinal hyperspectral imaging	leave-one-out cross-validation (LOOCV)	Classification: PD vs HC (Supra-nasal region)	Linear discriminant analysis	0.6	57.5% / -	60% / 55%	-
						Classification: PD vs HC (Inferonasal region)		0.6	55% / -	60% / 50%	-
Rupavath et al. (2024) (Rupavath et al., 2024)	-	-	-	retinal images from RIM-One and Drishti (Not-specified)	-	Classification: Neurodegenerative disorders (Not specified / RIM-One dataset)	ShAMBi-LSTM	-	96.5% / 99.2%	95.3% / -	- / 0.978
						Classification: Neurodegenerative disorders (Not specified / Drishti dataset)		-	97.2% / 99.5%	96.9% / -	- / 0.981

Hu et al. (2025) (Hu et al., 2025)	PD: 263	-	-	CFP	-	Classification: PD, MS, AMD, Glaucoma	FundusNet (CNN and vision transformer-based)	0.75	-	-	-
------------------------------------	---------	---	---	-----	---	---------------------------------------	--	------	---	---	---

2 *The extended abstract of this article, written in English, was included in our study. However, the accuracy, precision, sensitivity, and
3 specificity were reported in the main text study, but they were written in Chinese and, for this reason, were not included in the report.
4 **AD:** Alzheimer`s Disease, **AMD:** Age related macular degeneration, **CFP:** Color Fundus Photography, **CNN:** Convolutional Neural
5 Network, **GCL:** Ganglion Cell Layer, **HC:** Healthy Control, **KNN:** K-Nearest Neighbor, **LR:** Logistic Regression, **OCT:** Optic
6 Coherence Tomography, **OCTA:** Optic Coherence Tomography Angiography, **PD:** Parkinson`s disease, **RNFL:** Retinal Nerve Fiber
7 Layer, **RF:** Random Forest, **SVM:** Support Vector Machine, **UWF:** Ultra-Wide Field, **WMH:** White Matter Hyperintensity, **ShAMBi-**
8 **LSTM:** Shuffle Attention Mechanism depends on Bi-directional Long Short-Term Memory, **MS:** Multiple sclerosis, , **SGA:** selective-
9 guided adversarial network

10 The majority were classification studies (e.g., PD vs HC; PD vs atypical motor disorders; severity
11 grading such as Hoehn–Yahr scale or UPDRS-III) (Ahn et al., 2023; Álvarez-Rodríguez et al., 2024;
12 Chrysou et al., 2024; Hu et al., 2025; Jingqi Huang et al., 2024; Lee et al., 2023; Richardson et al., 2024;
13 Rupavath et al., 2024; Shi et al., 2024; Tran et al., 2024; Ueda et al., 2024), while others focused on retinal
14 layer segmentation (RNFL and/or GCL-BM, full-stack retinal segmentation) (Álvarez-Rodríguez et al.,
15 2024; Chen et al., 2024; Gende et al., 2023; Zhang et al., 2024; Zhao et al., 2021) and PD prediction (Hu et
16 al., 2022; Tran et al., 2024; Zhou et al., 2023). Across classification papers, AUC ranged from 0.6-0.918,
17 with a multimodal fundus/OCTA/Ultrawide field retinal imaging (UWF) model reaching the highest
18 accuracy; segmentation studies on macular OCT commonly achieved Dice 0.88–0.99 for GCL–BM, 0.90–
19 0.96 for RNFL, and full-retina Dice \approx 0.82–0.94.

20 **4. Discussion**

21 **4.1 Classification**

22 A support vector machine (SVM) is a ML algorithm used to identify hyperplanes and categorize
23 data into distinct groups (Cosma et al., 2017). SVM is mainly classified as a supervised learning model and
24 can perform linear and non-linear classifications (An et al., 2021; Mack, 2014; Winters-Hilt & Merat, 2007).
25 Nunes et al. (2019) (Nunes et al., 2019) used multiple non-linear SVM models to differentiate between
26 healthy controls (HC), AD, and PD. They included OCT images from a local dataset comprising 75
27 participants. The gray-level co-occurrence matrix was used for the feature extractor. In the next stage, each
28 SVM model was used as a binary classification between two of the three possible groups. Each model also
29 assessed each of the five retinal layers individually to make the diagnosis. They claim that excluding the
30 RNFL layer improved classification performance, and it was excluded. The best reported accuracy was
31 achieved with a five-fold cross-validation training model, ranging from 75.3% to 87.7% (median = 80.8%).
32 They also report that 94.4% (median; range: 88.9-96.6%; k=10) of diagnoses were correct when both eyes
33 of a participant received the same classification. In all scenarios, the model achieved the highest specificity

34 for PD and the highest sensitivity for HC, compared with AD. This finding may be due to the larger sample
35 sizes used for PD and HC compared with AD.

36 Temporal RNFL layer thickness correlates with functional PD scoring (Chang et al., 2022; Shafiee
37 et al., 2019). The correlation between retinal thickness and PD severity may be due to dopamine's role in
38 maintaining retinal thickness (Ahn et al., 2018; Svetel et al., 2025). Ahn et al. (2023) (Ahn et al., 2023)
39 developed five CNN models to differentiate PD from patients with atypical motor abnormalities. ResNet-
40 18 achieved the best results with an area under the curve (AUC) of 0.76 and an accuracy of 76.75%. Then,
41 they used the ResNet-18 model as a basis to predict H-Y scale and UPDRS-III (PD severity assessment)
42 scores from color fundus photography (CFP) and demographic data, including age, sex, hypertension status,
43 and diabetes status. For the H-Y stage (3-class), the best model (Model 4) achieved a sensitivity of 83.23%,
44 a specificity of 66.81%, an AUROC of 0.77, and an accuracy of 73.38% on internal data. For UPDRS-III
45 (3-class), Model 4 reached a sensitivity of 82.61% (81.38–83.83), a specificity of 65.75%, an AUROC of
46 0.77, and an accuracy of 71.64% on internal data. In the external H–Y test set, performance was sensitivity
47 70.73%, specificity 66.66%, AUROC 0.67, and accuracy 70.45%.

48 Álvarez-Rodríguez (2024) (Álvarez-Rodríguez et al., 2024) evaluated screening performance
49 across single-view (optic disc or macula) and multi-view (fusion of both) configurations, using F1-score as
50 the primary metric due to class imbalance for classification of PD from other neurological diseases. The
51 optic-disc single-view yields the weakest results, with PD F1 of approximately 0.50–0.6. Macular 2D
52 representations improved slightly. The strongest single-view performance is achieved by macular 3D
53 volume features, with PD F1 typically 0.70–0.80. Multi-view 2D (macula 2D + disc) sits around 0.60–0.70,
54 showing a gain over either 2D view alone but still below macula-3D. Multi-view 3D and 2D+3D fusion
55 generally matches macula-3D at ~0.70–0.80 with slightly lower variance rather than a consistent jump. In
56 short, the ranking is: macula-3D \gtrsim multi-view (3D or 2D+3D) > multi-view 2D > macula-2D \gg optic disc
57 only. An important innovation of this study is the combination of nnU-Net for segmentation, the DieT
58 feature extractor, and a histogram-based gradient-boosting classification tree for classification. Although

59 they don't compare their results with other combinations, properly concatenating multiple methods can
60 improve performance.

61 Lee et al. (2023) (Lee et al., 2023) utilized the AlexNet model to classify high- and low-quality
62 images in OCT and optical coherence tomography angiography (OCTA) images. The model trained on OCT
63 images achieved an AUC of 0.99. The superficial capillary plexus, identified from OCTA images, was also
64 used as an independent input to AlexNet, yielding an AUC of 0.832. The authors suggested that the better
65 AI performance in OCT may be due to the more accurate color maps used in OCT.

66 AI can detect and learn specific patterns in data and use them for classification. For example, PD
67 and primary open-angle glaucoma (POAG) both result in retinal thinning (Ullah et al., 2025). Chrysou et
68 al. (2024) (Chrysou et al., 2024) found that retinal layers, except retinal pigmented epithelium (RPE), were
69 thinner in POAG compared to PD. The difference was most significant in GCL thickness (26.4 μm vs. 34.8
70 μm), and the RPE thickness difference between POAG and PD was lowest (14.2 μm vs. 14 μm). Also,
71 when PD was compared to HC, the retina was thinner, and the difference was the greatest in the inner
72 plexiform layer (IPL) (34.2 μm vs. 36.1 μm) and the outer plexiform layer (OPL) (22.3 μm vs. 23.1 μm).
73 Subsequently, they trained a random forest (RF) model to distinguish between PD and POAG and between
74 PD and HC. RF randomly selects a feature from the data and then grows decision trees. The classification
75 is done based on the results of all grown decision trees (Salman et al., 2024). Chrysou et al.'s RF model
76 successfully identified the former layers (GCL, RPE, IPL, and OPL) as the best features in differentiating
77 PD from POAG and HC. The AUROC of the model in differentiating PD from POAG was higher than that
78 in differentiating PD from HC (0.92 vs. 0.71), which may be due to a greater thickness difference between
79 PD and POAG.

80 Richardson et al. (2024) (Richardson et al., 2024) used VGG-19 (a CNN-based algorithm) for
81 feature extraction from multiple retinal images, including OCT, OCTA, and UWF scanning laser
82 ophthalmoscopy. Four feature maps were generated by VGG-19 and then subjected to modality-specific
83 feature transformations to estimate PD probability and classify PD. The VGG-19 model was pretrained on

84 the ImageNet database, fine-tuned for PD, and applied in this research. The model trained on the left eye
85 performed best (AUC = 0.918), while the model trained on both eyes performed worst (AUC = 0.861).
86 Areas under the precision-recall curves for the left eye, the right eye, and both eyes were reported to be
87 0.677, 0.535, and 0.405. However, the authors emphasize that the 95% CIs for these models overlapped
88 substantially, so no statistically significant difference can be concluded for either the both-eyes vs single-
89 eye models or the left-eye-only vs right-eye-only models. The best performance was achieved when all
90 imaging modalities were used as inputs. The ultra-widefield color photography performed best, and the
91 GCL-IPL map performed worst when included as a single input.

92 Keke et al. (2024) (LIANG Keke, 2024) developed five different models to distinguish between
93 PD and HC. The logistic regression model achieved the highest AUC (0.841) compared to RF, Xception,
94 decision trees, and K-nearest neighbors. Shi et al. (2024) (Shi et al., 2024), introduced a retinal-structure-
95 guided CNN for early PD detection that combines 2 CNN methods (U-Net and Res-Net18). A U-Net first
96 segments 10 retinal layers on each OCT; these anatomy maps are then aligned and fused with early image
97 features, and a structure-guided attention module learns layer-specific weights so that PD-relevant layers
98 contribute more to the final decision. The whole system is trained end-to-end, embedding anatomical priors
99 directly into the classifier rather than relying solely on raw pixels. They employed two different five-fold
100 cross-validations: the eye-wise five-fold cross-validation yielded higher accuracy and precision (88.21% /
101 81.28%) compared to the subject-wise five-fold cross-validation (83.38% / 61.81%). Assigning a subject's
102 left and right eyes to different sets significantly affects PD recognition performance.

103 Rupavath et al. (2024) (Rupavath et al., 2024) extracted the gray-level co-occurrence matrix from
104 retinal pictures and used it to classify early neurodegenerative disease. This study employed the ShAM-Bi-
105 LSTM model, achieving accuracies of 96.5% and 97.2% in the RIM-One and Drishti databases,
106 respectively. This article does not specify the types of neurodegenerative diseases included. Additionally,
107 the databases used in this study may not be suitable for this research, as their primary focus is on non-
108 neurodegenerative diseases, such as glaucoma, and they include a sparse set of modalities. Still, they do not

109 specify which ones they actually used for training and testing (Chakravarty & Sivaswamy, 2017; Fumero
110 et al., 2011; Sivaswamy et al., 2014). Hu et al. (Hu et al., 2025) used several transformer-based and CNN
111 models and then employed ensemble methods for classification. Their combination employs Nfnet, RegNet,
112 and EfficientNet, alongside ViT methods (VOLO, XCIT, CIAT), as feature extractors, and multiple CNN
113 and ViT models, combined with ensemble techniques, as classifiers. This method resulted in an AUC of
114 0.75 for PD.

115 PD screening is not a routine practice in current medical care. However, with the introduction of
116 newer treatment options, screening and prophylaxis treatment may become available in the future.
117 WaveSRNet, introduced by Huang et al. [32], is an AI model designed for this purpose. This model aims to
118 preserve the high-frequency features while extracting low-frequency features and reducing image noise.
119 The RNFL, GCL-IPL, OPL, and outer nuclear layers were the main layers used by this algorithm for PD
120 screening. This method results in an AUC of 0.7516 and an accuracy of 74.49% in PD screening.
121 Visualization (Grad-CAM, SHAP) indicates the model attends to specific layers and fovea-centered
122 macular regions, supporting that PD-related changes are layer- and region-dependent rather than diffuse
123 (Veys et al., 2019).

124 While many models focus on using OCT, OCTA, or CFP for training AI models, Ueda et al. (2024)
125 (Ueda et al., 2024) used data of retinal hyperspectral imaging as input for linear discriminant analysis
126 (LDA). They hypothesized that α -synuclein accumulation in the retina can alter retinal light-scattering
127 properties. They observed that, at short wavelengths, retinal scattering differed with HC, especially in the
128 supra-nasal and inferonasal regions. The retinal reflectance spectra in both supra- and inferotemporal
129 regions of PD overlapped with HC and were not used for differentiation. This method yielded an AUC of
130 0.6 in classifying PD and HC. Although this study found the difference between PD and HC eyes to be in
131 the nasal section of the retina, most of the studies report that the temporal side is more affected in PD (Di
132 Pippo et al., 2023). However, some studies still report the nasal part to be more affected due to the PD

133 (Svetel et al., 2025). The observed overlap in retinal temporal regions may be due to the small sample size;
134 future studies can address this issue by increasing the number of participants.

135 The included studies have employed various ML and DL models in this section; the most common
136 are CNN-based algorithms. The direct comparison between models in this task is tricky. The models have
137 incorporated data from multiple databases, employed different approaches targeting specific membranes,
138 and compared PD across conditions. There may be substantial differences in data quality across studies,
139 and the features of each modality and layer affect overall performance. Model performance has also been
140 shown to vary when PD is compared to different conditions (Chrysou et al., 2024). Although some
141 extremely high performances observed in the studies may be due to overfitting (Álvarez-Rodríguez et al.,
142 2024; Lee et al., 2023). The CNN-based models, particularly nnU-Net (Álvarez-Rodríguez et al., 2024) and
143 AlexNet (Lee et al., 2023), achieved the highest AUC and accuracy; however, when studies with more than
144 200 PD patients were considered, ResNet-18 (Ahn et al., 2023) performed best.

145 **4.2. Segmentation**

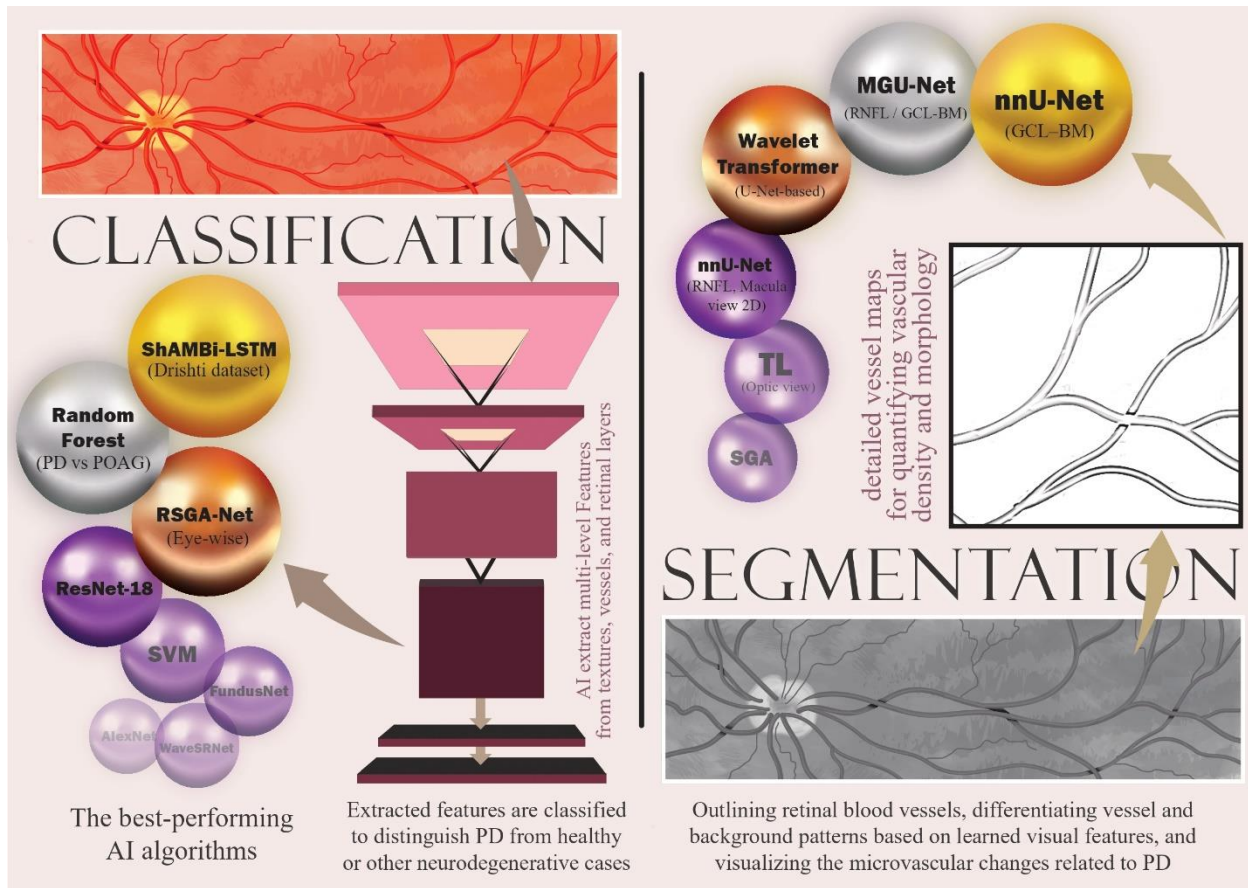
146 Context encoder network (CE-Net) is a DL algorithm proposed by Gu et al. (2019) (Gu et al., 2019)
147 for medical image segmentations. CE-Net segments 2D images using three main components: a feature
148 encoder, a content extractor, and a feature decoder. The encoder used in this model is a pre-trained ResNet-
149 34 architecture trained on the ImageNet dataset. The content extractor uses a dense atrous convolutional
150 block and a residual multi-kernel pooling block to minimize spatial data loss. Zhao et al. (2021) (Zhao et
151 al., 2021) used the CE-Net model for OCT image segmentation and determined the retinal layer thickness
152 changes in PD. They report that the interdigitation zone and retinal pigment epithelium-Bruch membrane
153 complex were thicker in PD compared to healthy controls. However, their study included only six
154 participants with PD and utilized a cross-sectional design.

155 The multi-scale GCN-assisted U-shape network (MGU-Net) was first developed by Li et al. (2021)
156 (Li et al., 2021). It aimed to segment retinal layers from OCT images in different patients using a U-Net-

157 based approach. This method was superior to similar algorithms, but it required that the input images be
158 standardized in a specific manner. Gende et al. (2023) (Gende et al., 2023) applied the MGU-Net to retinal
159 layer segmentation of different neurological diseases, including PD. The segmentation task is performed in
160 two stages: first, the retina is separated from background noise, and then the layers are identified. The best
161 PD performance was achieved by multi-disease training: leave-one-disease-out (train on other NDDs, test
162 on PD) yielded RNFL precision of 0.938 and GCL–BM precision of 0.984; pooling all diseases produced
163 essentially the same results. Training on a single disease and testing on PD yielded weaker results for RNFL
164 (precision of 0.930–0.946 with lower Dice scores), while GCL–BM remained near-ceiling (~0.983–0.989
165 Dice). The main limitation of this study is treating GCL-BM as a single complex, as in the study by Álvarez-
166 Rodríguez (Álvarez-Rodríguez et al., 2024).

167 They reported uniformly strong layer masks across views: on macula OCT, the RNFL dice score
168 was 0.955, whereas the GCL–BM score was near the ceiling at 0.985; moving from 2D to 3D macular
169 pipelines did not materially change these values. In the optic-disc view, RNFL dice was slightly lower
170 (0.90), whereas GCL–BM was 0.88. Transfer learning (TL) to the disc view primarily reduced training
171 time, yielding metrics comparable to those obtained by training from scratch.

172 Chen et al. (Chen et al., 2024), similar to Hu et al. (Hu et al., 2025), developed a WaveFormer that
173 combines two primary methods for image segmentation: CNN-based and Transformer-based segmentation.
174 They aim to build a model that can leverage both global context information via Transformer-based
175 segmentation and local information via CNNs. Their model used a U-Net architecture, with Transformer-
176 based segmentation during the contraction phase and convolution during the expansion phase. This method
177 achieved the highest Dice score (93.46%), accuracy (93.73%), and Intersection-over-Union (IoU)
178 (87.79%), and the lowest average 95% Hausdorff distance (2.63), compared with other models, such as U-
179 Net and Att-UNet. Figure 4 shows the best-performing AI algorithms for classification and segmentation
180 in PD detection.



181

182 **Figure 4.** Presentation of the top-performing AI models for classification and segmentation in PD detection.

183 It has been demonstrated that image quality can significantly impact the performance of AI models
 184 (Gong et al., 2023). Models that perform well on one dataset often show a significant drop in performance
 185 when tested on another. In clinical practice, even the device used to capture the image can affect data quality.
 186 Zhang et al. (2024) (Zhang et al., 2024) developed a segmentation algorithm trained on four devices and
 187 tested on three. A critical aspect of their model is that it aims to segment all retinal layers, rather than
 188 segmenting them into two sections: the RNFL and GCL-BM. Their SGA model achieved an IoU of 89.5%,
 189 a dice score of 94.43%, and a mean absolute error of 17.679 in segmenting the choroid layer of the eye. For
 190 complete retinal segmentation, it performed IoU, dice score, and mean absolute error of 70.62%, 82.48%,
 191 and 5.953, respectively. Segmenting only the outer retina yielded higher performance, with an IoU of
 192 78.23%, a dice score of 87.67%, and a mean absolute error of 4.038.

193 U-Net-based approaches are commonly used for image segmentation in patients with PD and
194 perform better on OCT images, particularly in identifying the RNFL layer. The addition of the Walvelt
195 spatial attention block or building model to a two-stage approach, such as MGU-Net, may further enhance
196 segmentation performance. The MGU-Net may achieve the best performance in this area due to the
197 background-removal stage precedes segmentation.

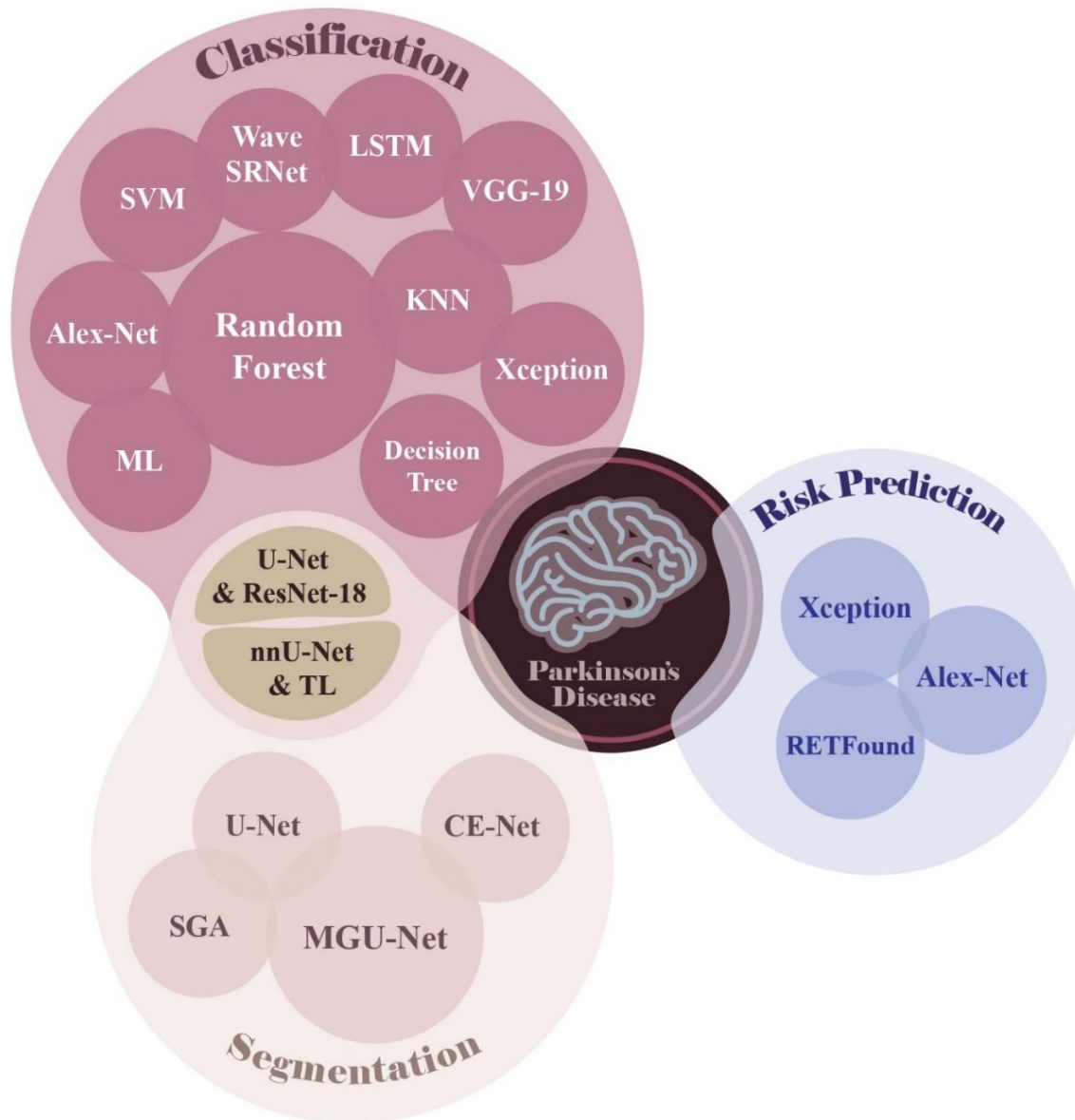
198 **4.3. PD Risk Prediction**

199 The retinal age gap, defined as the difference between deep learning predicted retinal age from
200 fundus photographs and chronological age, has emerged as a systemic risk signal; for example, Zhu et al.
201 (2022) (Zhu et al., 2023) showed that a positive retinal age gap is associated with higher all-cause mortality.
202 Building on this concept, Hu et al. (2022) (Hu et al., 2022) tested whether the retinal age gap predicts
203 incident Parkinson’s disease. The underlying rationale is that retinal tissue undergoes neurodegenerative
204 and vascular changes that parallel those in the brain; therefore, accelerated retinal ageing may signal an
205 elevated risk of PD. In the UK Biobank cohort of 35,834 PD-free participants (median follow-up 5.83 years;
206 63 incident PD), each 1-year increase in retinal age gap was associated with a 10% higher risk of developing
207 PD (hazard ratio 1.10, 95% CI 1.01–1.20; $p = 0.023$). Compared with the lowest quartile, the third quartile
208 had a hazard ratio of 2.66 (1.13–6.22), and the highest quartile had a hazard ratio of 4.86 (1.59–14.8). As a
209 5-year predictor, the retinal-age model achieved an AUROC of 0.708, similar to a simple risk-factor model
210 (0.717, not significantly different).

211 An article by Zhou et al. (2023) (Zhou et al., 2023) investigated the role of RETFound in PD
212 incidence prediction based on OCT and CFP images. They included 588 participants from the MEH-AlzEye
213 database for internal validation and 58 from the UK-Biobank for testing. They report an AUC of 0.669 for
214 PD prediction. Their algorithm also outperformed comparable AI models (SL-ImageNet, SSL-Image-Net,
215 SSL-Retina) when CFP images were used as input (P -value < 0.003). However, despite the higher
216 performance, the difference was not statistically significant when OCT images were used to predict PD

217 incidence ($P = 0.085$). They also observed that, in the internal dataset, RETFound outperformed CFP in
218 predicting PD incidence from OCT images.

219 To predict the prevalence and incidence of PD, Tran et al. (Tran et al., 2024), developed nine
220 different AI models. AlexNet achieved the best overall, incidence, and PD prevalence prediction
221 performance (AUC = 0.77, 0.68, and 0.73, respectively). Other AI algorithms (Logistic regression, VGG-
222 16, SVM, Elastic Net, Google-Net, Inception-V3, ResNet-50) achieved AUCs of 0.56-0.71, 0.56-0.73, and
223 0.54-0.64 in overall PD prediction, prevalence prediction, and incidence prediction, respectively. The
224 database used in this study is relatively small, which may affect the model's performance. Although the type
225 and quality of the data used differed between Tran et al. (Tran et al., 2024), and Zhou et al. (Zhou et al.,
226 2023), the AlexNet achieved a slightly better AUC compared to RETFound in PD incidence prediction. The
227 various AI architectures utilized in classification, segmentation, and PD risk assessment are illustrated in
228 Figure 5.



229

230 **Figure 5.** AI architectures applied for classification, segmentation, and PD risk assessment. For
 231 classification, the highest AUC was achieved with random forests, and the highest accuracy was achieved
 232 with ShAMBi-LSTM. The highest Dice score in segmentation was achieved with MGU-Net. The highest AUC risk
 233 prediction was achieved with Alex-Net

234 **4.4. Other Uses**

235 To reduce the data required to train AI models, Varghese et al. (2023) [24] used few-shot learning
 236 methods. Multiple few-shot approaches, such as TL, have been proposed; however, the technique used by
 237 Verghese et al. (2023) (Varghese et al., 2023) is called inductive logic programming (ILP). ILP logically

238 learns facts from background knowledge and from positive and negative examples (Kononenko & Kukar,
239 2007). The ILP uses these inputs to infer and generate a point, and then makes decisions based on that point.
240 Varghese et al. (2023) (Varghese et al., 2023) extracted histograms from patients' CFPs and used binning
241 methods to enable the ILP to learn them. The ILP models were then tested for the diagnosis of multiple
242 neurodegenerative diseases, including PD. The data presented in the figure demonstrate that ILP models,
243 especially the Meta Inverse Entailment (MIE)–PyGol, were superior to SVM, K-nearest neighbors, random
244 forests, and logical regression. The accuracy of Meta Inverse Entailment (MIE) – PyGol also rises as the
245 number of positive examples increases.

246 **5. Limitations and Future Direction**

247 **Study design:** Some studies have attempted to use longitudinal data to predict future risk of PD
248 development [52]; however, most studies employ a cross-sectional design, focusing on retinal segmentation
249 and PD/HC classification. Levodopa treatment affects the RNFL thickness in PD (Sen et al., 2014). RNFL
250 thickness can predict the future cognitive decline of PD (Zhang et al., 2021). These findings suggest that
251 retinal imaging may serve as a biomarker of disease progression and treatment response, and that
252 longitudinal studies can evaluate AI's performance in these tasks.

253 **Sample size and Datasets:** Only a few studies included more than 100 patients with PD (Ahn et
254 al., 2023; Chrysou et al., 2024; Lee et al., 2023; Varghese et al., 2023; Zhou et al., 2023). It is noteworthy
255 that the study by Hu et al. (Hu et al., 2022) used a large dataset, but, given its aim, no patients with PD were
256 included at baseline. Only a small number of studies have used large databases such as the UK Biobank
257 (Hu et al., 2025; Hu et al., 2022; Tran et al., 2024; Zhou et al., 2023) or iMIND (Lee et al., 2023). Other
258 databases used in the studies were MEH-MIDAS (Zhou et al., 2023), MEH-AlzEye (Zhou et al., 2023),
259 Heidelberg-SPECTRALIS (Álvarez-Rodríguez et al., 2024), and OCD-PD (Chen et al., 2024). Small
260 sample sizes in studies can significantly reduce model performance and increase model uncertainty (Riley
261 et al., 2025). The optimal sample size for each study should be calculated based on its specific setting. The
262 type of outcome, the number of predictor variables, the prevalence of the outcome in target individuals, the

263 desired margin of error, the desired shrinkage factor, and the signal-to-noise ratio (Riley et al., 2020).
264 PMASAMPSIZA and PMVALSAMPSIZE are Stata models proposed for calculating the minimum required
265 sample sizes for training and validation of models (Ensor, 2018, 2023; Riley et al., 2025). Using multiple
266 databases can increase sample size, but this should be done carefully to reduce bias during data integration
267 (Putrama & Martinek, 2024).

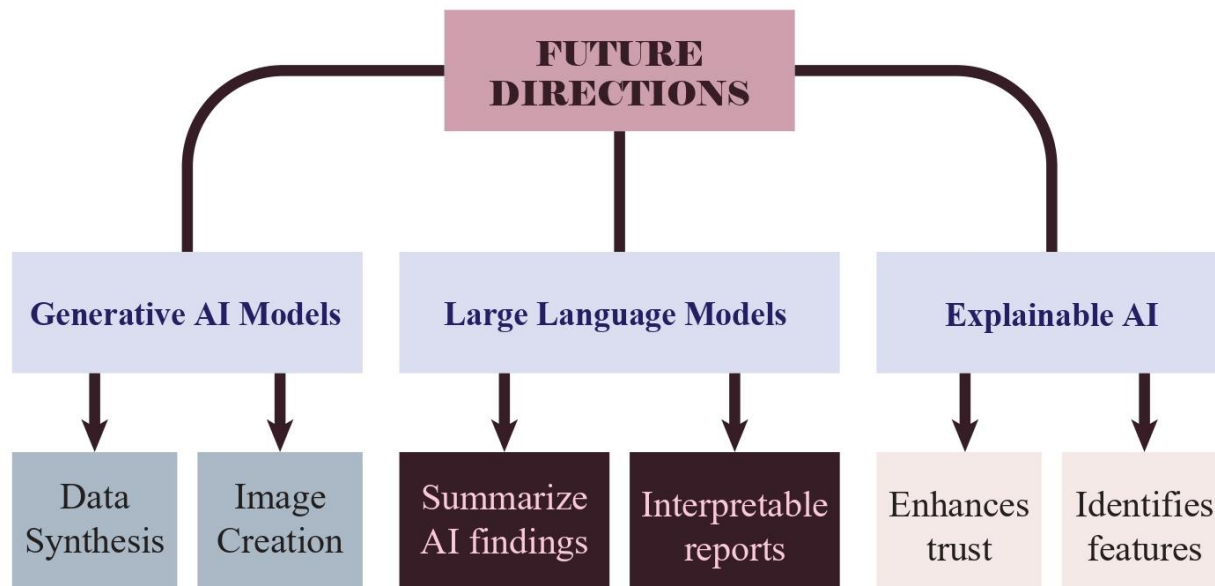
268 **Generative models:** Studies can also employ generative methods to artificially increase sample
269 size. These models can detect features and generate similar data that is indistinguishable from the original
270 ones (Reddy, 2024). The data can then be used to train an actual model. This way, studies can increase their
271 sample sizes with high-quality images while keeping costs to a minimum. Generative adversarial networks
272 (GANs) are among the most widely used generative AI models for data synthesis (Suthar et al., 2022).
273 Using these methodologies is reported to increase the accuracy compared to conventional models (Gulakala
274 et al., 2022). GANs are less frequently used in ophthalmology-related image generation than in other
275 medical fields. However, it has been demonstrated that GANs can generate high-quality OCT images useful
276 for educational purposes (Peng et al., 2024; Wang et al., 2021).

277 GANs are also used to create future CFPs for age-related macular degeneration from baseline
278 fundus images (Pham et al., 2022). In a study by Coronado et al. (Coronado et al., 2023) GAN recreated
279 OCTA images from CFP. This approach can effectively reduce the cost while maintaining high-quality data.
280 These results demonstrate that GANs can be effectively applied to retinal imaging research, including OCT,
281 OCTA, and CFP images. Although the use of generative models can improve performance, some reports
282 indicate that they have led to a decline (Riley et al., 2025). Thus, the authors need to apply them carefully.

283 **Transfer learning:** We also encourage testing the proposed models with other external data
284 sources. AI models tend to perform worse when presented with data that differs from the data on which
285 they were fine-tuned. Most studies used ImageNet as the source domain and medical images as the target
286 domain. ImageNet is an extensive database of mostly non-medical images (Deng et al., 2009). The
287 similarity between the source and target domains in TL-based training approaches can enhance AI

288 efficiency (Peng et al., 2022) and improve performance. Using PD-based databases as the source domain
289 and fine-tuning the models on local PD data may yield more accurate models.

290 **Explainable AI:** Using explainable AI (XAI) models can help identify the features the AI model
291 uses for its tasks. Only a few studies have used this method (Hu et al., 2025; Tran et al., 2024). However,
292 the study by Hu et al. (Hu et al., 2025) applied XAI to patients with PD. Using XAI models can enable
293 human operators to override AI results (Ali et al., 2023). Large language models (LLMs), such as ChatGPT,
294 can also help summarize and organize the findings of other AI models and prepare an interpretable report
295 (Parillo et al., 2024). In specific situations, LLMs have also demonstrated potential to generate plausible
296 answers when provided with sufficient clinical data (Gilson et al., 2023). Using XAI and LLMs can help
297 clinicians better understand the AI's reasoning and make models more user-friendly. However, these models
298 should be used with extreme caution, as there are reports of misdiagnoses, incorrect reports, and errors (de
299 Bruijn et al., 2022; Parillo et al., 2024). Future studies can integrate XAI and LLMs into the current
300 proposed methodologies for retinal imaging in PD and investigate their performance. Figure 6 summarizes
301 the proposed future directions.



302

303 **Figure 6.** Overview of the proposed future directions in AI-assisted retinal PD research.

304 6. Conclusion

305 In this review, we have summarized proposed AI models for detecting PD, segmenting the retina
306 in PD, enhancing image quality, predicting PD severity, and forecasting PD progression. Retinal thickness,
307 particularly the RNFL and GCL, is reduced in patients with PD. The former changes are observed early in
308 PD and can serve as valuable biomarkers for diagnosis. AI can segment retinal layers from OCT images or
309 use texture analysis of OCTA and CFP to predict PD from HC and other neurodegenerative diseases, such
310 as AD, WMH, and multiple sclerosis, as well as other diseases with Parkinsonian features. The performance
311 of AI models depends on many factors, such as sample size, database balance, use of TL, AI architecture,
312 imaging technology, image quality, task complexity, and the number of classification classes. AI shows
313 promising results in PD-related functions. However, the use of TL, XAI, and generative models can increase
314 the performance. Future research can elucidate the role of retinal imaging in PD progression and
315 prognostication using AI models trained on larger longitudinal datasets.

316 Abbreviations

317 **AD:** Alzheimer`s Disease, **AI:** Artificial intelligence, **AMD:** Age related macular degeneration, **AUC:** area
318 under the curve, **CE-Net:** Context encoder network, **CFP:** Color Fundus Photography, **CNN:**
319 Convolutional Neural Network, **CNS:** central nervous system, **DL:** Deep learning, **GANs:** Generative
320 adversarial networks, **GCC:** Ganglion cell complex, **GCL:** Ganglion Cell Layer, **GCL-IPL:** Ganglion cell
321 inner plexiform layer, **HC:** Healthy Control, **ILP:** inductive logic programming, **IPL:** inner plexiform
322 layer, **KNN:** K-Nearest Neighbor, **LDA:** linear discriminant analysis, **LLMs:** Large language models, **LR:**
323 Logistic Regression, **MGU-Net:** multi-scale GCN-assisted U-shape network, **MIE:** Meta Inverse
324 Entailment, **ML:** Machine learning, **MRI:** Magnetic resonance imaging, **MS:** Multiple sclerosis, **OCT:**
325 Optic Coherence Tomography, **OCTA:** Optic Coherence Tomography Angiography, **OPL:** outer plexiform
326 layer, **PD:** Parkinson`s disease, **POAG:** primary open-angle glaucoma, **RF:** Random Forest, **RNFL:**
327 Retinal nerve fiber layer, **RPE:** retinal pigmented epithelium, **SGA:** selective-guided adversarial network,
328 **ShAMBi-LSTM:** Shuffle Attention Mechanism depends on Bi-directional Long Short-Term Memory,

329 **SVM:** Support Vector Machine, **UPDRS:** Unified Parkinson’s Disease Rating Scale, **UWF:** Ultra-Wide
330 Field, **WMH:** White Matter Hyperintensity, **XAI:** explainable AI

331 **Declaration**

332 **Ethics approval and consent to participate:**

333 This study was conducted under the principles outlined in the Declaration of Helsinki.

334 **Consent for publication**

335 N/A

336 **Availability of data**

337 N/A

338 **Competing interests**

339 The authors declare that there is no conflict of interest.

340 **Funding Sources**

341 None.

342 **CRedit Statement**

343 **Conceptualization:** AJ **Data curation:** HA, MA, PK, and AJ **Investigation:** AJ, HA, PK, and MA

344 **Supervision:** RA, RT, RAS, and AJz **Visualization:** NS **Writing – original draft:** AJ, HA, MA, NS, and

345 RT **Writing – review & editing:** RT, RAS, AJ, and RA **Project administration:** AJ

346 It should be noted that AJ and HA are co-first authors, and AJ and RAS are co-corresponding authors of
347 this manuscript.

348

349 **Acknowledgments**

350 None.

351

352 **References**

353 Ahn, J., Lee, J.-Y., Kim, T. W., Yoon, E. J., Oh, S., Kim, Y. K., Kim, J.-M., Woo, S. J., Kim, K.
354 W., & Jeon, B. (2018). Retinal thinning associates with nigral dopaminergic loss in de

355 novo Parkinson disease. *Neurology*, 91(11), e1003-e1012.
356 <https://doi.org/doi:10.1212/WNL.0000000000006157>

357 Ahn, S., Shin, J., Song, S. J., Yoon, W. T., Sagong, M., Jeong, A., Kim, J. H., & Yu, H. G. (2023).
358 Neurologic Dysfunction Assessment in Parkinson Disease Based on Fundus Photographs
359 Using Deep Learning. *JAMA Ophthalmology*, 141(3), 234-240.
360 <https://doi.org/10.1001/jamaophthalmol.2022.5928>

361 Ali, S., Abuhmed, T., El-Sappagh, S., Muhammad, K., Alonso-Moral, J. M., Confalonieri, R.,
362 Guidotti, R., Del Ser, J., Díaz-Rodríguez, N., & Herrera, F. (2023). Explainable Artificial
363 Intelligence (XAI): What we know and what is left to attain Trustworthy Artificial
364 Intelligence. *Information Fusion*, 99, 101805.
365 <https://doi.org/https://doi.org/10.1016/j.inffus.2023.101805>

366 Álvarez-Rodríguez, L., Pueyo, A., de Moura, J., Vilades, E., Garcia-Martin, E., Sánchez, C. I.,
367 Novo, J., & Ortega, M. (2024). Fully automatic deep convolutional approaches for the
368 screening of neurodegeneratives diseases using multi-view OCT images. *Artif Intell Med*,
369 158, 103006. <https://doi.org/10.1016/j.artmed.2024.103006>

370 An, Y., Li, H., Su, T., & Wang, Y. (2021). Determining Uncertainties in AI Applications in AEC
371 Sector and their Corresponding Mitigation Strategies. *Automation in Construction*, 131,
372 103883. <https://doi.org/https://doi.org/10.1016/j.autcon.2021.103883>

373 Bayhan, H. A., Aslan Bayhan, S., Tanık, N., & Gürdal, C. (2014). The association of spectral-
374 domain optical coherence tomography determined ganglion cell complex parameters and
375 disease severity in Parkinson's disease. *Curr Eye Res*, 39(11), 1117-1122.
376 <https://doi.org/10.3109/02713683.2014.894080>

377 Chakravarty, A., & Sivaswamy, J. (2017). Joint Optic Disc and Cup Boundary extraction from
378 Monocular fundus images. *Computer Methods and Programs in Biomedicine*, 147.
379 <https://doi.org/10.1016/j.cmpb.2017.06.004>

380 Chang, Z., Xie, F., Li, H., Yuan, F., Zeng, L., Shi, L., Zhu, S., Lu, X., Wei, X., & Wang, Q.
381 (2022). Retinal Nerve Fiber Layer Thickness and Associations With Cognitive
382 Impairment in Parkinson's Disease [Original Research]. *Frontiers in Aging Neuroscience*,
383 Volume 14 - 2022. <https://doi.org/10.3389/fnagi.2022.832768>

384 Chen, Y., Zhang, X., Wang, T., Tang, C., Ye, H., & Liu, J. (2024, 30 June-5 July 2024).
385 WaveFormer: A Wavelet Transformer for Parkinson Disease's Retinal Layer
386 Segmentation in OCT. 2024 International Joint Conference on Neural Networks (IJCNN),
387 Chrysou, A., Heikka, T., van der Zee, S., Boertien, J. M., Jansonius, N. M., & van Laar, T.
388 (2024). Reduced Thickness of the Retina in de novo Parkinson's Disease Shows A
389 Distinct Pattern, Different from Glaucoma. *J Parkinsons Dis*, 14(3), 507-519.
390 <https://doi.org/10.3233/jpd-223481>

391 Coronado, I., Pachade, S., Trucco, E., Abdelkhaleq, R., Yan, J., Salazar-Marioni, S., Jagolino-
392 Cole, A., Bahrainian, M., Channa, R., Sheth, S. A., & Giancardo, L. (2023). Synthetic
393 OCT-A blood vessel maps using fundus images and generative adversarial networks.
394 *Scientific Reports*, 13(1), 15325. <https://doi.org/10.1038/s41598-023-42062-9>

395 Cosma, G., Brown, D., Archer, M., Khan, M., & Graham Pockley, A. (2017). A survey on
396 computational intelligence approaches for predictive modeling in prostate cancer. *Expert
397 Systems with Applications*, 70, 1-19.
398 <https://doi.org/https://doi.org/10.1016/j.eswa.2016.11.006>

399 de Bruijn, H., Warnier, M., & Janssen, M. (2022). The perils and pitfalls of explainable AI:
400 Strategies for explaining algorithmic decision-making. *Government Information*
401 *Quarterly*, 39(2), 101666. <https://doi.org/https://doi.org/10.1016/j.giq.2021.101666>

402 Deng, J., Dong, W., Socher, R., Li, L. J., Kai, L., & Li, F.-F. (2009, 20-25 June 2009). ImageNet:
403 A large-scale hierarchical image database. 2009 IEEE Conference on Computer Vision
404 and Pattern Recognition,

405 Di Pippo, M., Fragiotta, S., Di Staso, F., Scuderi, L., & Abdolrahimzadeh, S. (2023). The Role of
406 Alpha-Synuclein Deposits in Parkinson's Disease: A Focus on the Human Retina. *Int J*
407 *Mol Sci*, 24(5). <https://doi.org/10.3390/ijms24054391>

408 Elanwar, R., Al Masry, H., Ibrahim, A., Hussein, M., Ibrahim, S., & Masoud, M. M. (2023).
409 Retinal functional and structural changes in patients with Parkinson's disease. *BMC*
410 *Neurol*, 23(1), 330. <https://doi.org/10.1186/s12883-023-03373-6>

411 Ensor, J. (2018). *PMSAMPSIZE: Stata module to calculate the minimum sample size required for*
412 *developing a multivariable prediction model*. In *Statistical Software Components IDEAS*.
413 <https://ideas.repec.org/c/boc/bocode/s458569.html>

414 Ensor, J. (2023). *PMVALSAMPSIZE: Stata module to calculate the minimum sample size*
415 *required for external validation of a multivariable prediction model*. In *Statistical*
416 *Software Components IDEAS*. <https://ideas.repec.org/c/boc/bocode/s459226.html>

417 Fumero, F., Alayon, S., Sanchez, J. L., Sigut, J., & Gonzalez-Hernandez, M. (2011, 27-30 June
418 2011). RIM-ONE: An open retinal image database for optic nerve evaluation. 2011 24th
419 International Symposium on Computer-Based Medical Systems (CBMS),

420 Ganji, Z., Nikparast, F., Shoeibi, N., Shoeibi, A., Zare, H., & Sharak, N. A. (2025). Retinal
421 imaging and artificial intelligence: A systematic review and meta-analysis of diagnostic
422 techniques for neurodegenerative diseases. *Photodiagnosis and Photodynamic Therapy*,
423 55, 104788. <https://doi.org/https://doi.org/10.1016/j.pdpdt.2025.104788>

424 Gende, M., Mallen, V., de Moura, J., Cordon, B., Garcia-Martin, E., Sanchez, C. I., Novo, J., &
425 Ortega, M. (2023). Automatic Segmentation of Retinal Layers in Multiple
426 Neurodegenerative Disorder Scenarios. *IEEE J Biomed Health Inform*, 27(11), 5483-
427 5494. <https://doi.org/10.1109/jbhi.2023.3313392>

428 Gilson, A., Safranek, C. W., Huang, T., Socrates, V., Chi, L., Taylor, R. A., & Chartash, D.
429 (2023). How Does ChatGPT Perform on the United States Medical Licensing
430 Examination (USMLE)? The Implications of Large Language Models for Medical
431 Education and Knowledge Assessment. *JMIR Med Educ*, 9, e45312.
432 <https://doi.org/10.2196/45312>

433 Gong, Y., Liu, G., Xue, Y., Li, R., & Meng, L. (2023). A survey on dataset quality in machine
434 learning. *Information and Software Technology*, 162, 107268.
435 <https://doi.org/https://doi.org/10.1016/j.infsof.2023.107268>

436 Gu, Z., Cheng, J., Fu, H., Zhou, K., Hao, H., Zhao, Y., Zhang, T., Gao, S., & Liu, J. (2019). CE-
437 Net: Context Encoder Network for 2D Medical Image Segmentation. *IEEE Transactions*
438 *on Medical Imaging*, 38(10), 2281-2292. <https://doi.org/10.1109/TMI.2019.2903562>

439 Gulakala, R., Markert, B., & Stoffel, M. (2022). Generative adversarial network based data
440 augmentation for CNN based detection of Covid-19. *Scientific Reports*, 12(1), 19186.
441 <https://doi.org/10.1038/s41598-022-23692-x>

442 Heim, B., Krismer, F., De Marzi, R., & Seppi, K. (2017). Magnetic resonance imaging for the
443 diagnosis of Parkinson's disease. *J Neural Transm (Vienna)*, 124(8), 915-964.
444 <https://doi.org/10.1007/s00702-017-1717-8>

- 445 Hu, W., Li, K., Gagnon, J., Wang, Y., Raney, T., Chen, J., Chen, Y., Okunuki, Y., Chen, W., &
446 Zhang, B. (2025). FundusNet: A Deep-Learning Approach for Fast Diagnosis of
447 Neurodegenerative and Eye Diseases Using Fundus Images. *Bioengineering*, 12(1), 57.
448 <https://www.mdpi.com/2306-5354/12/1/57>
- 449 Hu, W., Wang, W., Wang, Y., Chen, Y., Shang, X., Liao, H., Huang, Y., Bulloch, G., Zhang, S.,
450 Kiburg, K., Zhang, X., Tang, S., Yu, H., Yang, X., He, M., & Zhu, Z. (2022). Retinal age
451 gap as a predictive biomarker of future risk of Parkinson's disease. *Age Ageing*, 51(3).
452 <https://doi.org/10.1093/ageing/afac062>
- 453 Huang, J., Zhang, X., Jin, R., Xu, T., Jin, Z., Shen, M., Lv, F., Chen, J., & Liu, J. (2024).
454 Wavelet-based selection-and-recalibration network for Parkinson's disease screening in
455 OCT images. *Comput Methods Programs Biomed*, 256, 108368.
456 <https://doi.org/10.1016/j.cmpb.2024.108368>
- 457 Huang, J., Zhang, X., Jin, R., Xu, T., Jin, Z., Shen, M., Lv, F., Chen, J., & Liu, J. (2024).
458 Wavelet-based selection-and-recalibration network for Parkinson's disease screening in
459 OCT images. *Computer Methods and Programs in Biomedicine*, 256, 108368.
- 460 Kobylecki, C. (2020). Update on the diagnosis and management of Parkinson's disease. *Clin Med*
461 *(Lond)*, 20(4), 393-398. <https://doi.org/10.7861/clinmed.2020-0220>
- 462 Kononenko, I., & Kukar, M. (2007). Chapter 4 - Knowledge Representation. In I. Kononenko &
463 M. Kukar (Eds.), *Machine Learning and Data Mining* (pp. 107-129). Woodhead
464 Publishing. <https://doi.org/https://doi.org/10.1533/9780857099440.107>
- 465 Lee, T., Rivera, A., Brune, M., Kundu, A., Haystead, A., Winslow, L., Kundu, R., Wisely, C. E.,
466 Robbins, C. B., Henao, R., Grewal, D. S., & Fekrat, S. (2023). Convolutional Neural
467 Network-Based Automated Quality Assessment of OCT and OCT Angiography Image
468 Maps in Individuals With Neurodegenerative Disease. *Transl Vis Sci Technol*, 12(6), 30.
469 <https://doi.org/10.1167/tvst.12.6.30>
- 470 Li, J., Jin, P., Zhu, J., Zou, H., Xu, X., Tang, M., Zhou, M., Gan, Y., He, J., Ling, Y., & Su, Y.
471 (2021). Multi-scale GCN-assisted two-stage network for joint segmentation of retinal
472 layers and discs in peripapillary OCT images. *Biomed Opt Express*, 12(4), 2204-2220.
473 <https://doi.org/10.1364/boe.417212>
- 474 LIANG Keke, G. Q., LI Xiaohuan, MA Jianjun, YANG Hongqi, SHI Xiaoxue, FAN
475 Yongyan, YANG Dawei, GUO Dashuai, DONG Linrui, GU Qi, LI Dongsheng.
476 (2024). Predictive Value of Machine Learning Based on Retinal Structural Changes for
477 Early Parkinson's Disease Diagnosis [Original Research]. *Chinese General Practice*,
478 27(9), 7. <https://doi.org/https://www.chinagp.net/EN/10.12114/j.issn.1007-9572.2023.045>
- 479 Luo, Y., Qiao, L., Li, M., Wen, X., Zhang, W., & Li, X. (2025). Global, regional, national
480 epidemiology and trends of Parkinson's disease from 1990 to 2021: findings from the
481 Global Burden of Disease Study 2021 [Original Research]. *Frontiers in Aging*
482 *Neuroscience, Volume 16 - 2024*. <https://doi.org/10.3389/fnagi.2024.1498756>
- 483 Mack, P. (2014). Chapter 35 - Big Data, Data Mining, and Predictive Analytics and High
484 Performance Computing. In L. E. Jones (Ed.), *Renewable Energy Integration* (pp. 439-
485 454). Academic Press. [https://doi.org/https://doi.org/10.1016/B978-0-12-407910-
486 6.00035-1](https://doi.org/https://doi.org/10.1016/B978-0-12-407910-6.00035-1)
- 487 Nunes, A., Silva, G., Duque, C., Januário, C., Santana, I., Ambrósio, A. F., Castelo-Branco, M.,
488 & Bernardes, R. (2019). Retinal texture biomarkers may help to discriminate between
489 Alzheimer's, Parkinson's, and healthy controls. *PLoS One*, 14(6), e0218826.
490 <https://doi.org/10.1371/journal.pone.0218826>

- 491 Parillo, M., Vaccarino, F., Beomonte Zobel, B., & Mallio, C. A. (2024). ChatGPT and radiology
492 report: potential applications and limitations. *Radiol Med*, *129*(12), 1849-1863.
493 <https://doi.org/10.1007/s11547-024-01915-7>
- 494 Peng, J., Xie, X., Lu, Z., Xu, Y., Xie, M., Luo, L., Xiao, H., Ye, H., Chen, L., Yang, J., Zhang,
495 M., Zhao, P., & Zheng, C. (2024). Generative adversarial networks synthetic optical
496 coherence tomography images as an education tool for image diagnosis of macular
497 diseases: a randomized trial. *Front Med (Lausanne)*, *11*, 1424749.
498 <https://doi.org/10.3389/fmed.2024.1424749>
- 499 Peng, M., Li, Z., & Juan, X. (2022). Similarity-based domain adaptation network.
500 *Neurocomputing*, *493*, 462-473.
501 <https://doi.org/https://doi.org/10.1016/j.neucom.2021.12.089>
- 502 Pham, Q. T. M., Ahn, S., Shin, J., & Song, S. J. (2022). Generating future fundus images for
503 early age-related macular degeneration based on generative adversarial networks.
504 *Computer Methods and Programs in Biomedicine*, *216*, 106648.
505 <https://doi.org/https://doi.org/10.1016/j.cmpb.2022.106648>
- 506 Putrama, I. M., & Martinek, P. (2024). Heterogeneous data integration: Challenges and
507 opportunities. *Data in Brief*, *56*, 110853.
508 <https://doi.org/https://doi.org/10.1016/j.dib.2024.110853>
- 509 Pyatigorskaya, N., Gallea, C., Garcia-Lorenzo, D., Vidailhet, M., & Lehericy, S. (2014). A
510 review of the use of magnetic resonance imaging in Parkinson's disease. *Ther Adv Neurol*
511 *Disord*, *7*(4), 206-220. <https://doi.org/10.1177/1756285613511507>
- 512 Reddy, S. (2024). Generative AI in healthcare: an implementation science informed translational
513 path on application, integration and governance. *Implementation Science*, *19*(1), 27.
514 <https://doi.org/10.1186/s13012-024-01357-9>
- 515 Richardson, A., Kundu, A., Henao, R., Lee, T., Scott, B. L., Grewal, D. S., & Fekrat, S. (2024).
516 Multimodal Retinal Imaging Classification for Parkinson's Disease Using a
517 Convolutional Neural Network. *Transl Vis Sci Technol*, *13*(8), 23.
518 <https://doi.org/10.1167/tvst.13.8.23>
- 519 Riley, R. D., Ensor, J., Snell, K. I. E., Archer, L., Whittle, R., Dhiman, P., Alderman, J., Liu, X.,
520 Kirton, L., Manson-Whitton, J., van Smeden, M., Moons, K. G., Nirantharakumar, K.,
521 Cazier, J.-B., Denniston, A. K., Van Calster, B., & Collins, G. S. (2025). Importance of
522 sample size on the quality and utility of AI-based prediction models for healthcare. *The*
523 *Lancet Digital Health*, *7*(6), 100857.
524 <https://doi.org/https://doi.org/10.1016/j.landig.2025.01.013>
- 525 Riley, R. D., Ensor, J., Snell, K. I. E., Harrell, F. E., Martin, G. P., Reitsma, J. B., Moons, K. G.
526 M., Collins, G., & van Smeden, M. (2020). Calculating the sample size required for
527 developing a clinical prediction model. *BMJ*, *368*, m441.
528 <https://doi.org/10.1136/bmj.m441>
- 529 Rupavath, R. V. S. S. B., Alsalami, Z., Rafikiran, S., Sheeba, B., & Kanth, E. T. V. R. (2024, 4-5
530 Dec. 2024). Shuffle Attention Mechanism Based Bi-Directional Long Short-Term
531 Memory for Detecting Neurodegenerative Disorders. 2024 4th International Conference
532 on Mobile Networks and Wireless Communications (ICMNBC),
- 533 Salman, H., Kalakech, A., & Steiti, A. (2024). Random Forest Algorithm Overview. *Babylonian*
534 *Journal of Machine Learning*, *2024*, 69-79. <https://doi.org/10.58496/BJML/2024/007>
- 535 Sari, E. S., Koc, R., Yazici, A., Sahin, G., & Ermis, S. S. (2015). Ganglion cell-inner plexiform
536 layer thickness in patients with Parkinson disease and association with disease severity

537 and duration. *J Neuroophthalmol*, 35(2), 117-121.
538 <https://doi.org/10.1097/wno.0000000000000203>

539 Sen, A., Tugcu, B., Coskun, C., Ekinci, C., & Nacaroglu, S. A. (2014). Effects of levodopa on
540 retina in Parkinson disease. *Eur J Ophthalmol*, 24(1), 114-119.
541 <https://doi.org/10.5301/ejo.5000338>

542 Shafiee, K., Iranmanesh, F., Sharifi, A., Saliminiya, N., & Dehesh, T. (2019). The Retinal Nerve
543 Fiber Layer Thickness is Related to Severity of Parkinson's Disease. *Journal of Kerman*
544 *University of Medical Sciences*, 26(6), 479-487.
545 <https://doi.org/10.22062/jkmu.2019.89577>

546 Shi, H., Wei, J., Jin, R., Peng, J., Wang, X., Hu, Y., Zhang, X., & Liu, J. (2024). Retinal structure
547 guidance-and-adaption network for early Parkinson's disease recognition based on OCT
548 images. *Computerized Medical Imaging and Graphics*, 118, 102463.
549 <https://doi.org/https://doi.org/10.1016/j.compmedimag.2024.102463>

550 Sivaswamy, J., Krishnadas, S. R., Joshi, G. D., Jain, M., & Tabish, A. U. S. (2014, 29 April-2
551 May 2014). Drishti-GS: Retinal image dataset for optic nerve head(ONH) segmentation.
552 2014 IEEE 11th International Symposium on Biomedical Imaging (ISBI),

553 Su, D., Cui, Y., He, C., Yin, P., Bai, R., Zhu, J., Lam, J. S. T., Zhang, J., Yan, R., Zheng, X., Wu,
554 J., Zhao, D., Wang, A., Zhou, M., & Feng, T. (2025). Projections for prevalence of
555 Parkinson's disease and its driving factors in 195 countries and territories to 2050:
556 modelling study of Global Burden of Disease Study 2021. *BMJ*, 388, e080952.
557 <https://doi.org/10.1136/bmj-2024-080952>

558 Suthar, A. C., Joshi, V., & Prajapati, R. (2022). A review of generative adversarial-based
559 networks of machine learning/artificial intelligence in healthcare. *Handbook of Research*
560 *on Lifestyle Sustainability and Management Solutions Using AI, Big Data Analytics, and*
561 *Visualization*, 37-56.

562 Svetel, M., Marić, G., Božić, M., Lazić, U., Milovanović, A., Jakšić, J., Petrović, I., Dimitrijević,
563 A., Knežević, M., & Pekmezović, T. (2025). Retinal Thickness in Patients with
564 Parkinson's Disease and Dopa Responsive Dystonia—Is There Any Difference?
565 *Biomedicines*, 13(5), 1227. <https://www.mdpi.com/2227-9059/13/5/1227>

566 Thrall, J. H., Li, X., Li, Q., Cruz, C., Do, S., Dreyer, K., & Brink, J. (2018). Artificial
567 Intelligence and Machine Learning in Radiology: Opportunities, Challenges, Pitfalls, and
568 Criteria for Success. *J Am Coll Radiol*, 15(3 Pt B), 504-508.
569 <https://doi.org/10.1016/j.jacr.2017.12.026>

570 Tran, C., Shen, K., Liu, K., Ashok, A., Ramirez-Zamora, A., Chen, J., Li, Y., & Fang, R. (2024).
571 Deep learning predicts prevalent and incident Parkinson's disease from UK Biobank
572 fundus imaging. *Scientific Reports*, 14(1), 3637. [https://doi.org/10.1038/s41598-024-](https://doi.org/10.1038/s41598-024-54251-1)
573 [54251-1](https://doi.org/10.1038/s41598-024-54251-1)

574 Ueda, E., Watanabe, M., Nakamura, D., Matsuse, D., Tanaka, E., Fujiwara, K., Hashimoto, S.,
575 Nakamura, S., Isobe, N., & Sonoda, K. H. (2024). Distinct retinal reflectance spectra
576 from retinal hyperspectral imaging in Parkinson's disease. *J Neurol Sci*, 461, 123061.
577 <https://doi.org/10.1016/j.jns.2024.123061>

578 UIAin, N., Shaikh, R. M., & Malik, T. G. (2025). Pattern of RNFL Damage in Early- and Late-
579 Stage Primary Open-Angle Glaucoma Using the Disc Damage Likelihood Scale and
580 Optical Coherence Tomography. *Turk J Ophthalmol*, 55(3), 127-133.
581 <https://doi.org/10.4274/tjo.galenos.2025.88834>

- 582 Van Den Eeden, S. K., Tanner, C. M., Bernstein, A. L., Fross, R. D., Leimpeter, A., Bloch, D. A.,
583 & Nelson, L. M. (2003). Incidence of Parkinson's Disease: Variation by Age, Gender, and
584 Race/Ethnicity. *American Journal of Epidemiology*, 157(11), 1015-1022.
585 <https://doi.org/10.1093/aje/kwg068>
- 586 Varghese, D., Bauer, R., & Tamaddoni-Nezhad, A. (2023, 2023//). Few-Shot Learning
587 of Diagnostic Rules for Neurodegenerative Diseases Using Inductive Logic
588 Programming. *Inductive Logic Programming*, Cham.
- 589 Veys, L., Vandenaabeele, M., Ortuño-Lizarán, I., Baekelandt, V., Cuenca, N., Moons, L., & De
590 Groef, L. (2019). Retinal α -synuclein deposits in Parkinson's disease patients and animal
591 models. *Acta Neuropathologica*, 137(3), 379-395. [https://doi.org/10.1007/s00401-018-](https://doi.org/10.1007/s00401-018-01956-z)
592 [01956-z](https://doi.org/10.1007/s00401-018-01956-z)
- 593 Wang, Z., Lim, G., Ng, W. Y., Keane, P. A., Campbell, J. P., Tan, G. S. W., Schmetterer, L.,
594 Wong, T. Y., Liu, Y., & Ting, D. S. W. (2021). Generative adversarial networks in
595 ophthalmology: what are these and how can they be used? *Curr Opin Ophthalmol*, 32(5),
596 459-467. <https://doi.org/10.1097/icu.0000000000000794>
- 597 Winters-Hilt, S., & Merat, S. (2007). SVM clustering. *BMC Bioinformatics*, 8 Suppl 7(Suppl 7),
598 S18. <https://doi.org/10.1186/1471-2105-8-s7-s18>
- 599 Zhang, J.-r., Cao, Y.-l., Li, K., Wang, F., Wang, Y.-l., Wu, J.-j., Pei, S.-f., Chen, J., Mao, C.-j., &
600 Liu, C.-f. (2021). Correlations between retinal nerve fiber layer thickness and cognitive
601 progression in Parkinson's disease: A longitudinal study. *Parkinsonism & Related*
602 *Disorders*, 82, 92-97. <https://doi.org/https://doi.org/10.1016/j.parkreldis.2020.11.025>
- 603 Zhang, J., Lu, C., Song, R., Zheng, Y., Hao, H., Meng, Y., & Zhao, Y. (2024). Self-Guided
604 Adversarial Network for Domain Adaptive Retinal Layer Segmentation. *IEEE*
605 *Transactions on Instrumentation and Measurement*, 73, 1-10.
606 <https://doi.org/10.1109/TIM.2024.3440388>
- 607 Zhao, Y., Zhao, J., Gu, Y., Chen, B., Guo, J., Xie, J., Yan, Q., Ma, Y., Wu, Y., Zhang, J., Lu, Q., &
608 Liu, J. (2021). Outer Retinal Layer Thickness Changes in White Matter Hyperintensity
609 and Parkinson's Disease [Original Research]. *Frontiers in Neuroscience*, Volume 15 -
610 2021. <https://doi.org/10.3389/fnins.2021.741651>
- 611 Zhou, Y., Chia, M. A., Wagner, S. K., Ayhan, M. S., Williamson, D. J., Struyven, R. R., Liu, T.,
612 Xu, M., Lozano, M. G., Woodward-Court, P., Kihara, Y., Allen, N., Gallacher, J. E. J.,
613 Littlejohns, T., Aslam, T., Bishop, P., Black, G., Sergouniotis, P., Atan, D., . . . Vision, C.
614 (2023). A foundation model for generalizable disease detection from retinal images.
615 *Nature*, 622(7981), 156-163. <https://doi.org/10.1038/s41586-023-06555-x>
- 616 Zhu, Z., Shi, D., Guankai, P., Tan, Z., Shang, X., Hu, W., Liao, H., Zhang, X., Huang, Y., Yu, H.,
617 Meng, W., Wang, W., Ge, Z., Yang, X., & He, M. (2023). Retinal age gap as a predictive
618 biomarker for mortality risk. *Br J Ophthalmol*, 107(4), 547-554.
619 <https://doi.org/10.1136/bjophthalmol-2021-319807>

620